Biocompatible and pH sensitive PLGA encapsulated MnO nanocrystals for molecular and cellular MRI

M. F. Bennewitz[1], M. K. Nkansah[1], T. L. Lobo[2], and E. M. Shapiro[1,2]
[1]Department of Biomedical Engineering, Yale University, New Haven, CT, United States, [2]Department of Diagnostic Radiology, Yale University School of Medicine, New Haven, CT, United States

INTRODUCTION: Inorganic manganese based particles are becoming attractive for molecular and cellular imaging, due to their ability to provide bright contrast on T_1 weighted MRI, as opposed to the dark contrast generated from iron based particles. These cores are insoluble in water, but will dissolve slowly in acidic conditions. It is well established that upon internalization into cells, nanoparticles (NPs) and microparticles (MPs) are shuttled to low pH compartments within the cells (*1, 2*). Therefore, bright contrast in manganese particle labeled cells is most likely due to the evolved Mn^{2+}, which has an r_1 of 7 $mM^{-1}s^{-1}$, as a result of slow dissolution within low pH endosomes. This is supported by recent studies on dissolution of inorganic manganese cores in low pH buffers giving rise to bright contrast on MR images. (*3*)

Here we propose a novel paradigm for utilizing MnO nanocrystals for molecular and cellular MRI by encapsulating MnO within poly(lactic-*co*-glycolic acid) (PLGA) NPs and MPs. We demonstrate how these particles have very low r_1 molar relaxivities as intact particles and elicit high r_1 molar relaxivities upon dissolution in acidic media. The magnitude of the change in MRI properties is as high as 35-fold, making it the most dynamic 'smart' MRI contrast agent yet reported.

MATERIALS AND METHODS: Uniform MnO nanocrystals were synthesized by controlled thermal decomposition of manganese (II) acetylacetonate. PLGA NPs and MPs containing MnO cores were fabricated with a single emulsion technique. Fluorescence was incorporated into the particles thorough the addition of coumarin-6. Weight percents of MnO to PLGA during fabrication were 0%, 50% and 100%. MnO cores and particles were characterized by powder x-ray diffraction (XRD), transmission electron microscopy (TEM), and scanning electron microscopy (SEM). Total manganese content of the particles was investigated by thermal gravimetric analysis (TGA). r_1 molar relaxivities of intact 100% w/w MnO NPs and MPs suspended in agarose were determined at 4.0 Tesla.

To measure the longitudinal MRI properties of dissolving particles, NPs and MPs were suspended in PBS pH 7.4 and 20 mM sodium citrate pH 5, which mimic the cytosolic and endosomal cellular compartments, respectively. Mn^{2+} concentrations were calculated from the T_1 values of supernatants, collected at desired time points over 41 days, using a measured r_1 for Mn^{2+} of 7 $mM^{-1}s^{-1}$. The ability of NPs and MPs to label cells was assessed through addition of 20 µl of 5 mg/ml coumarin-6 doped, fluorescent MnO NP and MP solutions in media to confluent culture dishes of rat RG2 cells. Control cells received only growth medium. After a 24-hour incubation, cells were washed to remove free particles, trypsinized, and centrifuged to form a pellet. The subsequent pellets were then assessed by MRI at 4.0 Tesla to generate T_1 and R_1 values or analyzed by dual bright field and green fluorescence microscopy to analyze the extent of particle endocytosis.

RESULTS and DISCUSSION: TEM of MnO cores show 15-20 nm aggregates of several 5-10 nm cores. XRD confirmed the crystal structure and molecular identity of MnO nanocrystals. Average NP and MP diameters determined from SEM images (Figure 1A,B) were 140 $\pm$ 50 nm and 1.7 $\pm$ 0.9 µm, respectively. TEM of the intact PLGA encapsulated 100% w/w MnO NPs and MPs showed that MnO nanocrystals were distributed throughout both the NPs and MPs. Total manganese content of the particles ranged from 35% to 63% for the various formulations. Intact MnO NPs and MPs had very low r_1 of 0.21 $mM^{-1}s^{-1}$ and 0.54 $mM^{-1}s^{-1}$, respectively. This is due to the lack of direct contact water molecules have with the nanocrystals, as the nanocrystals are hydrophobic in nature and likely still capped with oleic acid.

To assess the dissolution characteristics of the particles, a controlled release experiment was performed. Particles in the citrate buffer pH 5 showed significant release of Mn^{2+} over 41 days, whereas, particles incubated in PBS pH 7.4 did not (Figure 2). In addition, the release of Mn^{2+} from NPs was faster than MPs, due to their higher surface area to volume ratio. To study dissolution of particles within cells, MnO NPs and MPs were incubated with RG2 cells for 24 hours and evaluated for labeling and evolved T_1 MRI contrast. After 24 hours, both NPs and MPs had successfully labeled RG2 cells with green fluorescence (Figure 3A,B). T_1 maps of control and labeled cell pellets were acquired at 4 Tesla (Figure 3C). The T_1 values of all the labeled cells were reduced compared to the control. Therefore, R_1 was increased after incubation of particles with the cells (Table 1) in the following order: 50% MnO MP < 50% MnO NP = 100% MnO MP < 100% MnO NP. These results can be explained through the controlled release experiment, which showed that NPs released Mn^{2+} at a faster rate than MPs. In addition, the 100% particle formulations contained more encapsulated MnO than the 50% formulations, and were able to cumulatively release more Mn^{2+}, resulting in a larger increase in R_1.

The agents reported here are 'smart' contrast agents, having environmentally sensitive properties. The conversion of MnO in acidic environments to Mn^{2+} yielded a maximal change in r_1 of 0.21 $mM^{-1}s^{-1}$ to 7 $mM^{-1}s^{-1}$, or nearly 35-fold. In general, however, the dynamic range of the change in molar relaxivity of other agents in response to biological or chemical stimuli is low. For example, EgadMe, the most recognizable 'smart' MRI contrast agent exhibits a 3-fold increase in r_1 following enzymatic activation (*4*). Various other 'smart' contrast agents designed to sense ions similarly exhibit 2.5 to 3-fold increases in r_1 (*5, 6*) The change in r_1 reported here is 10-fold higher than previously reported 'smart' contrast agents and are the most dynamic 'smart' contrast agents ever reported. The slow releasing Mn^{2+} formulations discussed here can be applied to liver imaging, targeting and visualization of tumors, and verification of cell endocytosis.

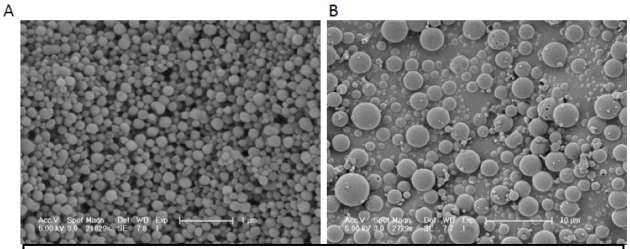

Figure 1, SEM of MnO A) NPs and B) MPs.

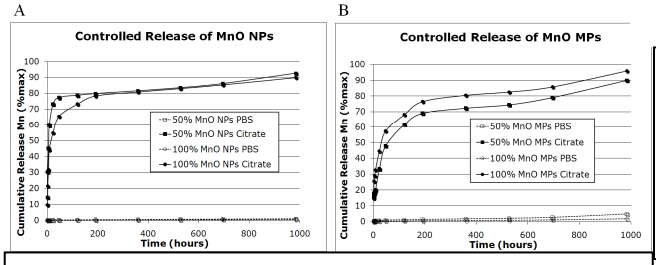

Figure 2, Controlled release of MnO A) NPs and B) MPs in PBS pH 7 (dashed lines) and 20 mM citrate pH 5 (solid lines). Cumulative release of Mn^{2+} is shown as % release over time for a total of 41 days.

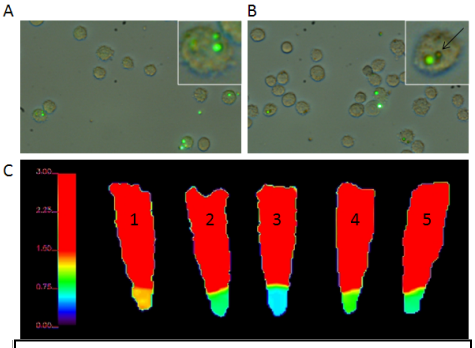

Figure 3, Bright field and fluorescence microscopy of RG2 cells labeled with A) 50% MnO MPs and B) 100% MnO MPs. C) T_1 maps of control and labeled RG2 cell pellets. From left to right: 1) unlabeled RG2 cells, 2) 50% MnO NPs, 3) 100% MnO NPs, 4) 50% MnO MPs, and 5) 100% MnO MPs.

Particle Type	T_1 (s)	R_1 (s^{-1})
None	1.29	0.78
50% MnO NPs	0.805	1.24
100% MnO NPs	0.594	1.68
50% MnO MPs	1.02	0.98
100% MnO MPs	0.805	1.24

Table 1: T_1 and R_1 for control and labeled RG2 cell pellets

References: 1. K. A. Hinds *et al.*, *Blood* **102**, 867 (2003). 2. A. S. Arbab *et al.*, *NMR Biomed.* **18**, 383 (2005). 3. E. M. Shapiro, A. P. Koretsky, *Magn Reson. Med.* **60**, 265 (2008). 4. A. Y. Louie *et al.*, *Nat. Biotechnol.* **18**, 321 (2000). 5. W. H. Li, *et al.*, *Inorg. Chem.* **41**, 4018 (2002). 6. J. L. Major, *et al.*, *PNAS* **104**, 13881 (2007).
NIH grants P30 NS052519 and DP2 OD004362